JOURNAL OF REINFORCED PLASTICS & COMPOSITES

Original article

Journal of Reinforced Plastics and Composites
2019, Vol. 38(21–22) 959–973

DOI: 10.1177/0731684419862350
journals.sagepub.com/home/jrp
SAGE

Buckling surrogate-based optimization framework for hierarchical stiffened composite shells by enhanced variance reduction method

Kuo Tian[1], Jiaxin Zhang[2], Xiangtao Ma[1], Yuwei Li[1], Yu Sun[1] and Peng Hao[1]

Abstract

The surrogate-based optimization of hierarchical stiffened composite shells against buckling is a typical multimodal and multivariables optimization problem. To improve the computational efficiency and global optimizing ability of the surrogate-based optimization of hierarchical stiffened composite shells, an enhanced variance reduction method based on Latinized partially stratified sampling and multifidelity analysis methods is proposed in this paper and then integrated into the surrogate-based optimization framework. In the offline step of the optimization framework, candidate pairing strategies of design variables are generated by Latinized partially stratified sampling and compared by performing priori optimizations based on the low-fidelity analysis method, and the optimal pairing strategy is therefore determined. On the basis of the optimal pairing strategy, the surrogate-based optimization is carried out using the high-fidelity analysis method in the online step. With less computational cost in the offline step, the proposed enhanced variance reduction method overcomes the limitation of Latinized partially stratified sampling that the optimal pairing strategy is not obvious in complex problems. Then, extensive optimization examples are carried out to verify the efficiency and effectiveness of the proposed optimization framework. Given an approximate computational cost, the optimal buckling result of the proposed framework using enhanced variance reduction method increases by 18.2% than that of the traditional framework based on Latin hypercube sampling. In particular, the advantage of enhanced variance reduction method in the space-filling ability is highlighted in comparison to Latin hypercube sampling. When achieving an approximate global optimal solution, the proposed framework reduces the total computational cost by 76.3% than the traditional framework. Finally, the numerical implementation of asymptotic homogenization method is used herein for the accurate prediction of effective stiffness coefficients of the initial design and optimal results. Through comparison, it is concluded that the high axial stiffness and bending stiffness are the main mechanism for the high load-carrying capacity of optimal results.

Keywords

Shell buckling, surrogate-based optimization, enhanced variance reduction method, multifidelity analysis

Introduction

As a typical thin-walled structure, stiffened shells have been widely used in launch vehicles and space shuttles.[1–4] Buckling is the major failure mode for shell structures under the axial compression load.[5,6] Many researchers are devoting to develop and design innovative configurations for stiffened shells,[7–19] in order to increase the structural load-carrying capacity. The hierarchical concepts of biological structures would be enlightening for the design of innovative

[1]Department of Engineering Mechanics, State Key Laboratory of Structural Analysis for Industrial Equipment, Dalian University of Technology, Dalian, China
[2]Department of Civil Engineering, Johns Hopkins University, Baltimore, MD, USA

Corresponding author:
Kuo Tian, Department of Engineering Mechanics, Dalian University of Technology, Dalian 116024, China.
Email: tiankuo@uw.edu

stiffened shells. For example, the dragonfly wing is one typical hierarchical structure with high specific stiffness, including brawny major veins to bear axial load and close-knit minor veins to resist local deformation.[20] Inspired by this, Wang et al.[21] developed novel hierarchical stiffened shells with diverse stiffener sizes and patterns, which improved the ability of stiffened shells against buckling and imperfections. Generally, the hierarchical stiffened shell is composed of the skin, major stiffeners (with larger sizes), and minor stiffeners (with smaller sizes).[22–29] The typical buckling modes for hierarchical stiffened shells are the global buckling mode, the partial global buckling mode (happens between the adjacent major stiffeners), skin local buckling mode, stiffener local buckling mode, and plastic buckling mode.[25] In order to investigate the outstanding load-carrying capacity of hierarchical stiffened panels, numerical and experimental studies have been carried out by Quinn et al.,[30–32] and corresponding design guidelines of hierarchical stiffened panels were also given by Houston et al.[33] Wang et al.[21] developed a novel hierarchical stiffened shell reinforced by orthogrid major stiffeners and triangle minor stiffeners and Zhao et al.[24] developed a novel one reinforced by triangle major and minor stiffeners, which both improved the bucking loads of stiffened shells significantly. Under the same weight, the hierarchical stiffened shell was verified to have low imperfection sensitivity in comparison to the traditional stiffened shell by Wang et al.[22] and Sim et al.[34,35] Additionally, the thermal buckling capacity of hierarchical stiffened structures was discussed by Wang et al.[36]

Although the hierarchical stiffened shell achieves higher load-carrying capacity than the traditional stiffened shell, its optimization problem is more complicated. Generally, the optimization of hierarchical stiffened shells faces two major challenges. The first challenge is the low analysis efficiency caused by the complicated and substantial local minor stiffeners, which result in tiny and detailed characteristics in finite element model. In order to accurately capture the pre-buckling path, the collapse point, and the post-buckling path, the explicit dynamic method would be a good choice because it can provide a more robust and stable analysis for the nonlinear behavior and it has a good agreement with the experimental results.[37–39] The explicit dynamic method has been extensively used to evaluate the collapse load for stiffened panels,[40] stiffened shells,[41–43] and hierarchical stiffened shells.[21,22] However, the computational time of the explicit dynamic method heavily relies on the element number and size, which results in the low computational efficiency of the buckling analysis of hierarchical stiffened shells. In this case, Wang et al.[21] smeared the minor stiffeners by means of asymptotic homogenization method, which reduced the post-buckling analysis time of hierarchical stiffened shells based on the detailed finite element method (FEM) by 84%. Wang et al.[25] proposed a fast prediction method (numerical-based smeared stiffener method, NSSM) for predicting the linear buckling load and mode of hierarchical stiffened shells. Based on NSSM, Wang et al.[25] further developed an adaptive equivalent strategy for hierarchical stiffened shells, which can obtain the equivalent model for hierarchical stiffened shells adaptively according to the critical buckling mode result predicted by NSSM. By combining proper orthogonal decomposition method with eigenvalue buckling method, Tian et al.[44] established a fast prediction method for buckling load and buckling mode of shell structures. Efficient reduced-order Koiter analysis methods were developed by Liang et al.[45,46] for shell structures, which can provide excellent accurate predictions for the post-buckling load and knockdown factors. Sun et al.[47] established an effective computational method to calculate buckling load results for grid-stiffened shells under compressive and thermal loads. The second challenge for the optimization of hierarchical stiffened shells is the low global optimizing ability caused by multimodal and multiple design variables of hierarchical stiffened shells. In comparison to the traditional stiffened shell, the hierarchical stiffened shell has more design variables, which results in a higher dimensional design space and thus challenges the ability of the optimization algorithm to find the global optimal solution. Wang et al.,[22] Hao et al.,[23] and Zhao et al.[24] pointed out that the genetic algorithm (GA) optimization method based on the surrogate modeling technique is an effective method to solve the global optimization problem of hierarchical stiffened shells. Zhao et al.[24] proposed a surrogate-based optimization framework for hierarchical triangle stiffened shells using the radial basis function (RBF) surrogate model, and the optimal hierarchical grid design contributed to avoiding the undesired local buckling. Based on the fixed-point method, Wang et al.[25] established a multilevel surrogate-based optimization framework by decomposing the entire optimization into a major-level sub-optimization and a minor-level sub-optimization, which can obtain a better global optimal solution than the single-level surrogate-based optimization method. Tian et al.[48] developed the competitive sampling method to tailor the global optimal design of hierarchical stiffened shells. Recently, the multifidelity modeling technology has contributed to improving the prediction accuracy and computational efficiency of surrogate-based optimizations.[49,50]

Sampling methods play a critical role on the performance of surrogate-based optimizations. An effective sampling method would contribute to describing the

design space more accurately and finding the global optimal solution more potentially. As one of the most common methods, Latin hypercube sampling (LHS) has been widely used for design of experiments,[51] Monte Carlo simulations,[52,53] and uncertainty quantification,[54–56] employed in nearly every field of computational engineering and science. Stein[57] showed that LHS can filter the variance associated with the additive components (main effects) of a transformation, which states that the main effects and low-order interactions are perhaps to govern the most general transformations and it leads LHS to reduce variance significantly. The "parent" methodology of LHS, stratified sampling (SS) has been attractive in the financial mathematics due to its capability to partition a population into strata that can be weighted based on their conditional probability. Some recent studies[58] proposed the "true" SS method wherein all dimensions of the space are stratified simultaneously. It differs from LHS in that it lies the opposite side such that each dimension of the random vector is stratified individually. Shields and Zhang[59] recently developed a generalized sampling method that is referred to as partially stratified sampling (PSS), which are proven to reduce variance associated with low-dimensional variable interactions, while LHS reduces variance associated with the main effects. To reduce the variance associated with the main-effects and low-dimensional interactions, Shields and Zhang[59] further proposed Latinized partially stratified sampling (LPSS), which combines the PSS method with Latinized stratified sampling (LSS) that produces sample sets that are simultaneously SS and LHS. LPSS achieves a considerable improvement in sampling efficiency by combining the effect of variance reductions of both PSS and LSS, particularly in high dimension. Several numerical examples and engineering applications[59] have been provided to highlight the good performance of LPSS on variance reduction in high dimension compared with other sampling methods. Nevertheless, Shields and Zhang[59] pointed out that one of the limitations of LPSS is that the optimal pairing of variables may not be obvious in complex problems. In this case, some engineering experiences or expert opinions are used to determine the optimal pairing of variables;[59] however, it is obvious that these methods are not reliable and could result in suboptimal results or bad results. In order to perform an efficient and effective global optimization for hierarchical stiffened shells, there is a strong demand to develop a strategy to guide the reasonable determination of the optimal pairing of variables for LPSS.

This outline of this paper is arranged as follows. In the upcoming section, the procedure of LPSS is introduced briefly, and then it is combined with multifidelity analysis methods to generate the enhanced variance reduction method (EVRM). Based on EVRM, the buckling surrogate-based optimization framework is established for hierarchical stiffened shells. Next, extensive illustrative examples are carried out to verify the effectiveness of the proposed optimization framework. Furthermore, detailed comparisons between optimal results of the proposed framework and traditional optimization frameworks are made from the viewpoint of computational efficiency and global optimizing ability. Finally, conclusions are made in the last section.

Methodology

Brief introduction of Latinized partially stratified sampling

According to Shields and Zhang,[59] the basis procedure of LPSS is summarized in Figure 1. The interested reader can find more details and discussions in Shields and Zhang.[59] In order to make LPSS easier to understand, we use the example of hierarchical stiffened composite shells to briefly introduce the basic procedure of LPSS.

The schematic diagram of the hierarchical stiffened composite shell is shown in Figure 2. The hierarchical stiffened composite shell has nine design variables composed of four discrete variables (includes the number of axial major stiffeners N_{aj}, the number of circumferential major stiffeners N_{cj}, the number of axial minor stiffeners between axial major stiffeners N_{an}, and the number of circumferential minor stiffeners between circumferential major stiffeners N_{cn}) and five continuous variables (includes the skin thickness t_s, the major stiffener height h_{rj}, the minor stiffener height h_{rn}, the major stiffener thickness t_{rj}, and the minor stiffener thickness t_{rn}).

From the point of view of geometrical characteristics, the hierarchical stiffened composite shell can be divided into three parts, including the skin, major stiffeners, and minor stiffeners. Following this point of view, we can decompose the nine-dimensional overall domain into subdomain $\Omega = \{[t_s], [h_{rj}, t_{rj}, N_{aj}, N_{cj}], [h_{rn}, t_{rn}, N_{an}, N_{cn}]\}$, which represent variables belonging to the skin, major stiffeners, and minor stiffeners, respectively. Thus, $\Omega_1 = 1$, $\Omega_2 = 4$, and $\Omega_3 = 4$. The strata for each subdomain is $\boldsymbol{S} = \{S_1, S_2, S_3\}$. According to the procedure of LPSS, the total number of LPSS points should satisfy this relationship, $N_t = {S_1}^{\Omega 1} = {S_2}^{\Omega 2} = {S_3}^{\Omega 3}$. In this case, if S_2=3, S_3 should be 3, and S_1 should be 81. Thus, the total number N_t is 81. Once all samples in subdomain are generated, a partially mapping strategy is implemented to assemble the full nine-dimensional samples $\boldsymbol{X} = \{t_s, h_{rj}, t_{rj}, N_{aj},$

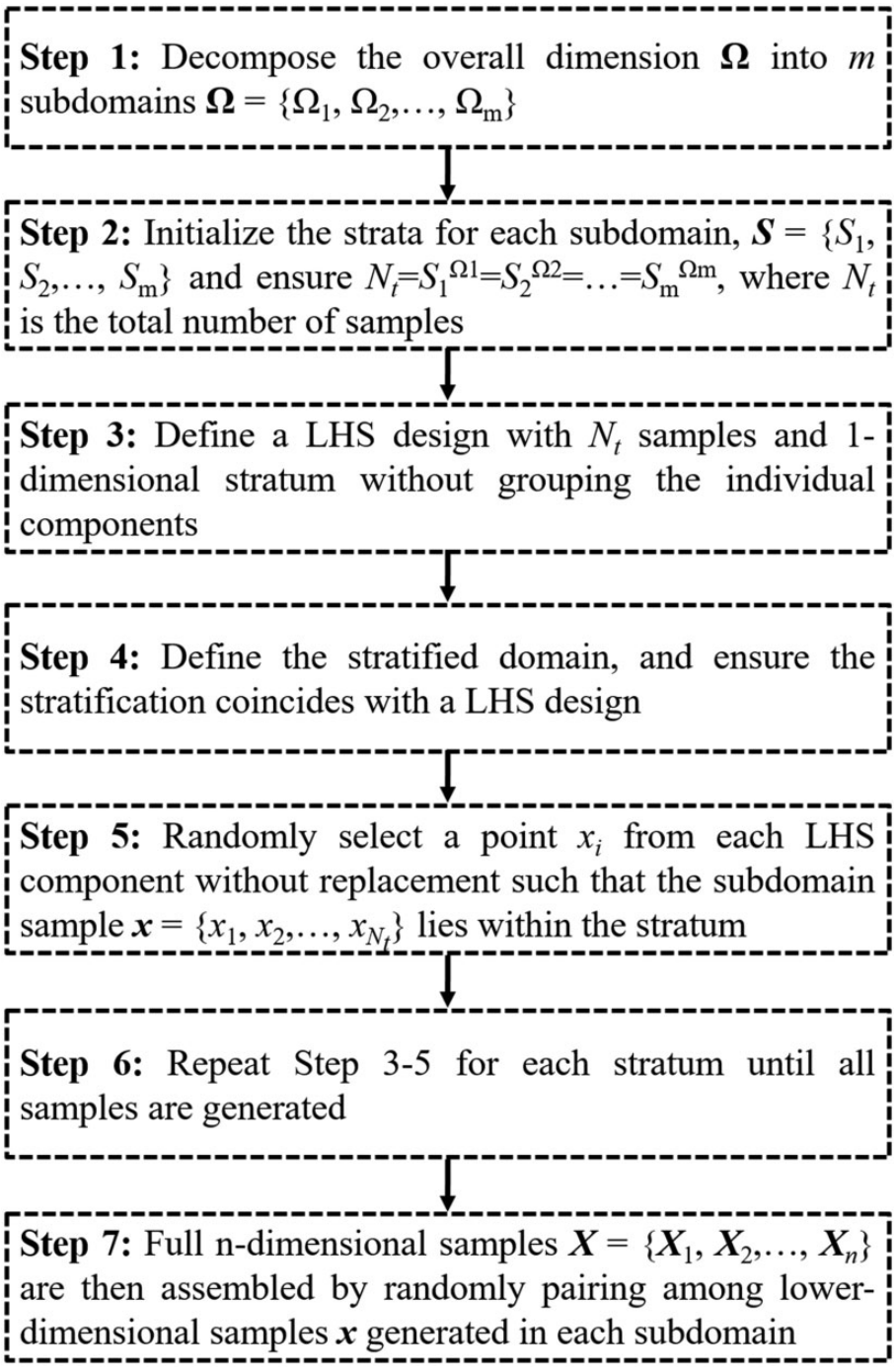

Figure 1. Basic procedure of LPSS.

N_{cj}, h_{rn}, t_{rn}, N_{an}, N_{cn}} by randomly pairing among samples in each subdomain.

This pairing strategy is referred to as candidate pairing strategy 1. According to the geometrical and physical characteristics of hierarchical stiffened composite shells, we can also obtain other representative candidate pairing strategies as presented in equation (1). One advantage of the LPSS method is to deal with the variable interaction effect, such as multiplicative relationship of variables ($a \times b$). We therefore arrange the variables with the multiplicative relationship into the same group. Following this, candidate pairing strategy 1 divides the domain into three subdomains {[t_s], [h_{rj}, t_{rj}, N_{aj}, N_{cj}], [h_{rn}, t_{rn}, N_{an}, N_{cn}]}

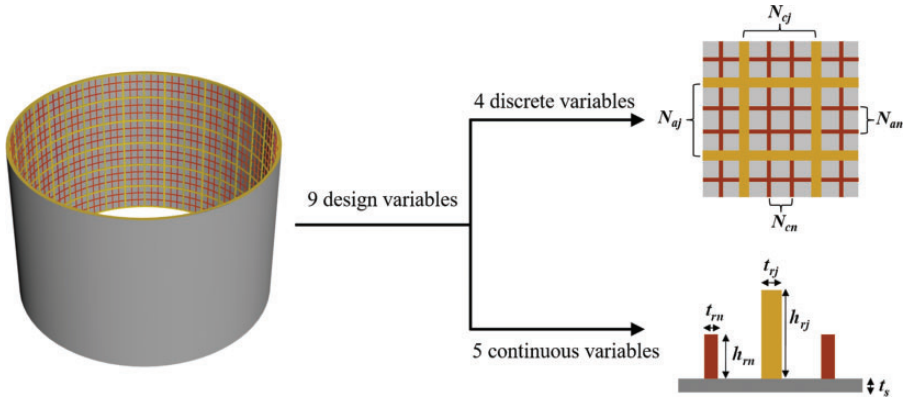

Figure 2. Schematic diagram of the hierarchical stiffened composite shell.

according to design variables belonging to the skin, major stiffeners, and minor stiffeners. Furthermore, we find that h_{rj} and t_{rj} have strong multiplicative relationship and their product stands for the cross-sectional area of major stiffeners (similarly, the product of h_{rn} and t_{rn} stands for the cross-sectional area of minor stiffeners), and N_{aj} and N_{cj} have a strong multiplicative relationship and their product stands for the total number of major stiffeners including axial and circumferential major stiffeners (similarly, the product of N_{an} and N_{cn} stands for the total number of minor stiffeners). As a result, the subdomain $[h_{rj}, t_{rj}, N_{aj}, N_{cj}]$ can be further classified into $[h_{rj}, t_{rj}]$ and $[N_{aj}, N_{cj}]$, and the subdomain $[h_{rn}, t_{rn}, N_{an}, N_{cn}]$ can be further divided into $[h_{rn}, t_{rn}]$ and $[N_{cj}, N_{cn}]$, which is referred to as candidate pairing strategy 2. In terms of the variable types of hierarchical stiffened composite shells, we thus divide the variables into two subdomains, including $[t_s, h_{rj}, t_{rj}, h_{rn}, t_{rn}]$ (continuous type) and $[N_{aj}, N_{an}, N_{cj}, N_{cn}]$ (discrete type). Note that, in the subdomain of $[t_s, h_{rj}, t_{rj}, h_{rn}, t_{rn}]$, t_s has relatively weak multiplicative relationship with other variables, so this subdomain can be further divided into $[t_s]$ and $[h_{rj}, t_{rj}, h_{rn}, t_{rn}]$. In this case, Candidate pairing strategy 3 has three subdomains, including $[t_s]$, $[h_{rj}, t_{rj}, h_{rn}, t_{rn}]$, and $[N_{aj}, N_{an}, N_{cj}, N_{cn}]$. It is noticed that N_{aj} and N_{an} have strong multiplicative relationship and their product stands for the total number of axial stiffeners including axial major stiffeners and axial minor stiffeners (similarly, the product of N_{cj} and N_{cn} stands for the total number of circumferential stiffeners). As mentioned above, h_{rj} and t_{rj} also have strong multiplicative relationship and their product stands for the cross-sectional area of major stiffeners (similarly, the product of h_{rn} and t_{rn} stands for the cross-sectional area of minor stiffeners). In this case, the subdomains of candidate pairing strategy 3 can be further divided into four subdomains, including $[t_s]$, $[h_{rj}, t_{rj}]$, $[h_{rn}, t_{rn}]$, $[N_{aj}, N_{an}]$, and $[N_{cj}, N_{cn}]$, which is referred to as candidate pairing strategy 4.

$$\begin{aligned}
&\text{Candidate pairing strategy 1 :}\\
&\quad [t_s],\ [h_{rj}, t_{rj}, N_{aj}, N_{cj}],\ [h_{rn}, t_{rn}, N_{an}, N_{cn}]\\
&\text{Candidate pairing\ strategy 2 :}\\
&\quad [t_s],\ [h_{rj}, t_{rj}],\ [h_{rn}, t_{rn}],\ [N_{aj}, N_{cj}],\ [N_{an}, N_{cn}]\\
&\text{Candidate pairing strategy 3 :}\\
&\quad [t_s],\ [h_{rj}, t_{rj}, h_{rn}, t_{rn}],\ [N_{aj}, N_{an}, N_{cj}, N_{cn}]\\
&\text{Candidate pairing strategy 4 :}\\
&\quad [t_s],\ [h_{rj}, t_{rj}],\ [h_{rn}, t_{rn}],\ [N_{aj}, N_{an}],\ [N_{cj}, N_{cn}]
\end{aligned} \tag{1}$$

Buckling surrogate-based optimization framework of hierarchical stiffened composite shells based on EVRM

In order to provide a reasonable determination method of the optimal pairing strategy of design variables for LPSS, the EVRM is established by combining LPSS with multifidelity analysis methods, and then EVRM is integrated into the surrogate-based optimization framework.

The flow chart of the buckling surrogate-based optimization framework based on EVRM is shown in Figure 3. It is divided into the offline low-fidelity analysis step and the online high-fidelity analysis step. Its key idea is to use the efficient low-fidelity analysis method to determine the optimal pairing strategy for LPSS, and then enhance the global optimizing ability of surrogate-based optimizations based on high-fidelity analysis methods. In this paper, NSSM is used as the low-fidelity analysis method of hierarchical stiffened composite shells, which was introduced in Wang et al.[25] The steps of NSSM are described as

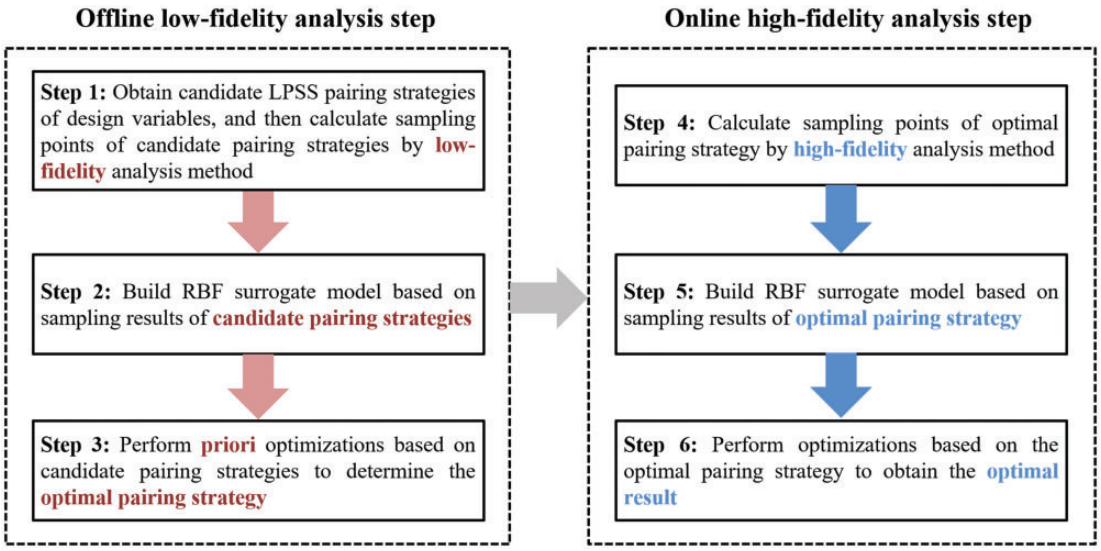

Figure 3. Flow chart of the buckling surrogate-based optimization framework based on EVRM.

follows: Firstly, the FE model of the repeating unit cell (RUC) of hierarchical stiffened composite shells is built. Then, the NIAH method is employed to predict the effective stiffness coefficients of RUC by analyzing the FE model. Finally, these effective stiffness coefficients are introduced into the Rayleigh–Ritz method to obtain the buckling load of hierarchical stiffened composite shells. Generally, NSSM needs about 6 s for single calculation. More details about NSSM can be found in Wang et al.[25] Furthermore, the explicit dynamic method is used as the high-fidelity analysis method of hierarchical stiffened composite shells in this paper, which can capture the collapse load of hierarchical stiffened composite shells.[21] For single calculation, the explicit dynamic method needs about 1.5 h.

In Step 1, according to the geometrical or physical characteristics of hierarchical stiffened composite shells, design variables are divided into different groups and those with strong interactions are paired in the same group, and thus several candidate pairing strategies are generated. Next, sampling points of candidate pairing strategies are calculated based on the low-fidelity analysis method.

In Step 2, RBF surrogate models are built based on sampling results of candidate pairing strategies in sequence.

In Step 3, priori surrogate-based optimizations are carried out based on candidate pairing strategies in sequence. After comparing optimal results of priori optimizations corresponding to candidate pairing strategies, the optimal pairing strategy achieving the highest buckling load is chosen from candidate pairing strategies. The optimization formulations are as follows

$$\begin{aligned} &\text{Find}: X = \left[t_s, h_{rj}, t_{rj}, N_{aj}, N_{cj}, h_{rn}, t_{rn}, N_{an}, N_{cn}\right] \\ &\text{Maximize}: P_{cr} \\ &\text{Subject to}: W \leq W^0 \end{aligned} \tag{2}$$

where $\boldsymbol{X}$ is referred to as the design variables, including t_s, h_{rj}, h_{rn}, t_{rj}, t_{rn}, N_{aj}, N_{cj}, N_{an}, N_{cn}. P_{cr} is the linear buckling load predicted by low-fidelity analysis method. The optimization objective is to maximize the linear buckling load P_{cr}, subject to the constraint that the structural weight W is not larger than the initial value W^0. The surrogate-based optimization is composed of the inner optimization and the outer update. The inner optimization is performed using global optimization algorithm, such as multi-island genetic algorithm (MIGA).[60] Then, the optimal result obtained from the surrogate-based optimization is validated by the corresponding detailed model simulation. The relative percentage error between two results is chosen as the convergence criterion, to decide whether the outer update is implemented to improve the prediction accuracy of the surrogate model. The update criterion is achieved by adding the optimal solution simulated from the high-fidelity model into the original surrogate model. Until the relative percentage error is less than 1.0%, the entire optimization is finally completed.

Steps 1 to 3 belong to the offline low-fidelity analysis step, which can determine the optimal LPSS pairing

strategy with less computational cost. They should be finished before performing the online high-fidelity analysis step.

In Step 4, sampling points of the optimal pairing strategy are calculated based on the high-fidelity analysis method.

In Step 5, the RBF surrogate model is built based on the sampling result from the optimal pairing strategy.

In Step 6, the surrogate-based optimization is performed based on the optimal pairing strategy. The optimization formulations are as follows

$$\begin{aligned} &\text{Find}: X = \left[t_s, h_{rj}, t_{rj}, N_{aj}, N_{cj}, h_{rn}, t_{rn}, N_{an}, N_{cn}\right] \\ &\text{Maximize}: P_{co} \\ &\text{Subject to}: W \leq W^0 \end{aligned} \tag{3}$$

where P_{co} is the collapse load predicted by the high-fidelity analysis method. The optimization objective is to maximize the collapse load P_{co}, subject to the constraints where the structural weight W is not larger than the initial value W^0. Similar with Step 3, the surrogate-based optimization in Step 6 is also composed of the inner optimization and the outer update.

Illustrative example

Model description for hierarchical stiffened composite shells

The hierarchical stiffened composite shell model is established with identical geometrical parameters and boundary conditions as described in literature,[21–23] as shown in Figure 2. The diameter D of the hierarchical stiffened composite shell is 3000 mm, and the length L of the hierarchical stiffened composite shell is 2000 mm. The geometrical parameters are listed in Table 1, including N_{aj}, N_{cj}, N_{an}, N_{cn}, t_s, h_{rj}, h_{rn}, t_{rj}, and t_{rn}. The material used for the hierarchical stiffened composite shell is SiC particle reinforced Al matrix (SiC/Al) composites. SiC/Al composites have achieved outstanding excellent combination of multifunctional properties inclusive of high thermal conductivity, low tailorable coefficient of thermal expansion, and high modulus and, thus, they are considered as one type of potential composite materials used in aerospace fields.[61–63] The isotropic mechanical properties of SiC/Al composites are as follows: Young's modulus $E = 100{,}000$ MPa and Poisson's ratio $\upsilon = 0.3$. The structural weight W^0 of the initial design is 369 kg. The boundary condition of the hierarchical stiffened composite shell is to keep the lower end of the hierarchical stiffened composite shell clamped and the upper end fixed except the degrees of freedom along the axial direction. A uniform axial load is applied to the upper end of the hierarchical stiffened composite shell. In this study, a workstation with a CPU of Intel Xeon E5-2687w @ 3.10 GHz and 64G RAM is used.

Optimal results of the traditional optimization framework based on LHS method

The traditional surrogate-based optimization method used in literature[21–23] generates sampling points using the LHS method, and then establishes the RBF surrogate model to perform the optimization. In order to verify the prediction accuracy of the surrogate models, the leave-one-out cross-validation method mentioned in Rikards et al.[64] is carried out in the design space. As pointed out by Myers et al.,[65] R^2 value can be used as an effective method to evaluate the prediction accuracy of surrogate models. Its formulation is as follows

$$R^2 = 1 - \frac{\sum_{i=1}^{j} (y_i - \hat{y}_i)^2}{\sum_{i=1}^{j} (y_i - \tilde{y}_i)^2} \tag{4}$$

where j is the total number of sampling points, y_i is the actual value of the ith sampling point, $\hat{y}_i$ is the predicted value by surrogate models, and $\tilde{y}_i$ is the mean

Table 1. The design space and optimal results of optimizations based on LHS and EVRM.

	t_s (mm)	t_{rj} (mm)	t_{rn} (mm)	h_{rj} (mm)	h_{rn} (mm)	N_{cj}	N_{cn}	N_{aj}	N_{an}	W (kg)	P_{co} (kN)	CPU time (h)
Initial design	2.9	5.0	10.0	26.0	13.0	8	4	35	2	369	19824	–
Lower bound	2.5	3.0	3.0	15.0	6.0	3	1	20	1	–	–	–
Upper bound	5.5	12.0	12.0	30.0	15.0	9	4	50	4	369	–	–
Optimization I-1 (81 LHS points)	5.0	5.5	3.8	21.2	12.5	4	2	50	3	362	22,680	124
Optimization I-2 (100 LHS points)	4.8	4.0	7.9	29.6	10.5	3	3	50	2	365	23,915	178
Optimization I-3 (200 LHS points)	5.1	6.6	3.3	25.0	14.8	3	2	50	2	368	24,693	345
Optimization I-4 (300 LHS points)	5.3	5.0	8.4	25.6	9.5	5	1	50	1	368	25,578	510
Optimization I-5 (400 LHS points)	4.1	8.3	3.9	30.0	15.0	4	2	50	2	364	25,683	702
Optimization V-1 (81 LPSS points)	5.4	4.6	3.6	30.0	15.0	5	1	50	1	367	26,804	121

value of the actual values of all sampling points. The more R^2 approximates to 1.0, the more accurate the surrogate model is. The R^2 results of surrogate models are listed in Table 2. It can be found that the established surrogate models have high prediction accuracy, and thus the surrogate models are credible.

A total of 81 LHS sampling points are used to carry out the surrogate-based optimization, referred to as Optimization I-1 in this paper. Its optimal collapse load is 22,680 kN, which is listed in Table 1. In comparison to the initial design (19,824 kN), the optimal collapse load (22,680 kN) of Optimization I-1 increases by 14.4%. To fully explore the global optimizing ability, more LHS sampling points (100, 200, 300, and 400 sampling points) are drawn, and the corresponding surrogate-based optimizations are carried out, which are referred to as Optimization I-2, Optimization I-3, Optimization I-4, and Optimization I-5, respectively. Corresponding optimal results are listed in Table 1. With the increase of the sample size in optimizations, the optimal collapse load gradually increases and converges to 25,683 kN when the number of sampling points reaches 400. The converged optimal collapse load (25,683 kN) increases by 29.6% compared with the initial design (19824 kN). Along with the improvement of the global optimizing ability of the surrogate-based optimization, the total computational time increases from 124 h to 702 h sharply, indicating a huge additional computational cost. The calculated results are summarized in Figure 4.

Optimal results of the proposed optimization framework based on EVRM

According to Figure 3, the proposed optimization framework based on EVRM is carried out. In the off-line low-fidelity analysis step, candidate LPSS pairing strategies of design variables are fully discussed.

Herein, optimizations based on candidate pairing strategy 1, candidate pairing strategy 2, candidate pairing strategy 3, and candidate pairing strategy 4 are referred to as Optimization II-1, Optimization III-1, Optimization IV-1, and Optimization V-1, respectively. In order to make the comparison clearer, totally 81 LPSS sampling points are generated for Optimization II-1, Optimization III-1, Optimization IV-1, and Optimization V-1. The corresponding LPSS subdomains are {1, 4, 4}, {1, 2, 2, 2}, {1, 4, 4}, and

Table 2. R^2 results of surrogate models of optimizations.

	Optimization I-1 (81 LHS points)	Optimization I-2 (100 LHS points)	Optimization I-3 (200 LHS points)	Optimization I-4 (300 LHS points)	Optimization I-5 (400 LHS points)	Optimization V-1 (81 LPSS points)
R^2 of P_{co}	0.94	0.95	0.97	0.99	0.98	0.97
R^2 of W	0.97	0.98	0.99	0.99	0.99	0.98

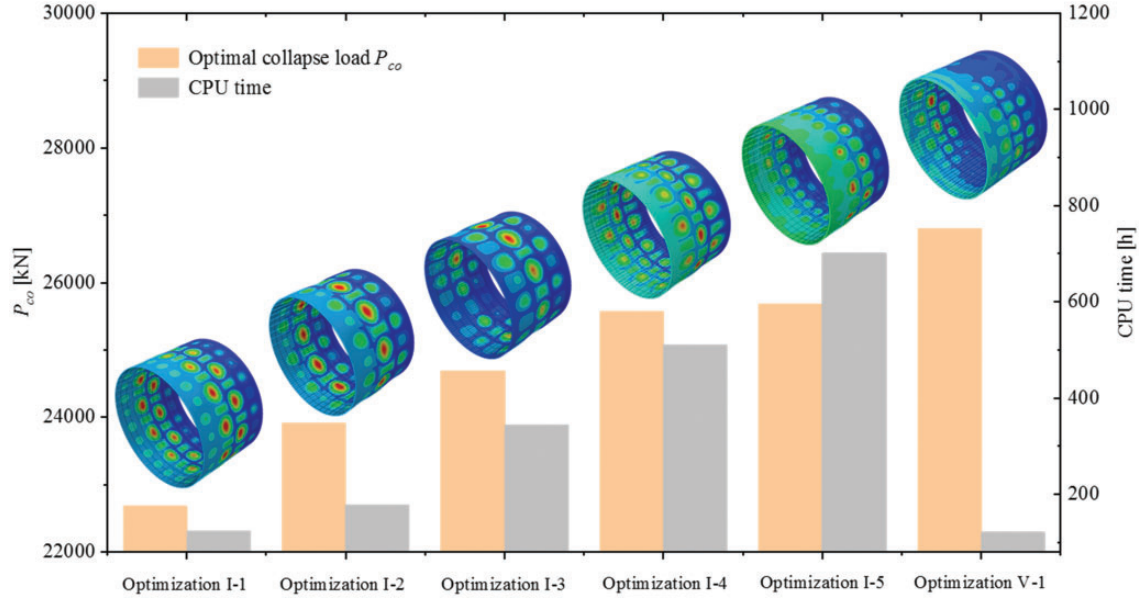

Figure 4. Comparisons of optimal collapse load and CPU time for optimization results.

{1, 2, 2, 2} respectively, and the corresponding LPSS strata for each subdomain are {81, 3, 3}, {81, 9, 9, 9}, {81, 3, 3}, and {81, 9, 9, 9} respectively.

Next, four prior optimizations are carried out based on candidate pairing strategies, with optimal linear buckling results listed in Table 3. It is evident that Optimization V-1 achieves the highest buckling load, and thus its pairing strategy is considered as the optimal pairing strategy among candidate pairing strategies. Furthermore, the optimal number of sampling points of the optimal pairing strategy is investigated. Optimization V-1 contains 81 LPSS sampling points, and 64 and 100 LPSS sampling points are generated for Optimization V-2 and Optimization V-3, respectively. Similarly, prior optimizations are carried out for Optimization V-2 and Optimization V-3, with optimal results shown in Table 3. By comparing Optimization V-1, Optimization V-2, and Optimization V-3, we can find that, as the number of LPSS sampling points increases, the optimal linear buckling load gradually increases and converges when the number of sampling points reaches 81. In this case, Optimization V-1 with 81 LPSS sampling points is considered to the optimal pairing strategy from the point of view of global optimizing ability and computational efficiency. Owing to using the low-fidelity analysis method, the offline low-fidelity analysis step only needs 0.9 h, which provides a reasonable pairing strategy for LPSS with less computational cost.

Then, in the online high-fidelity analysis step, the surrogate-based optimization is carried out for Optimization V-1. The optimal result is listed in Table 1. By comparison, Optimization V-1 achieves the best optimal result than other results of optimization based on LHS, which verifies the effectiveness of the optimal pairing strategy determined from the offline low-fidelity analysis step. The optimal collapse load (26,804 kN) of Optimization V-1 increases by 35.2% than the initial design (19824 kN). Costing the approximate computational time (both use 81 sampling points), the optimal collapse load (26,804 kN) of Optimization V-1 increases by 18.2% than the result (22,680 kN) of Optimization I-1, indicating the huge advantage of EVRM than the traditional LHS method. In order to obtain the global optimal solution, the optimization based on LHS needs 300 LHS points (Optimization I-4). By contrast, the optimization based on EVRM only needs 81 LPSS points (Optimization V-1) to achieve the global optimal solution, which significantly reduces the total computational time of Optimization I-4 (510 h) by 76.3%. Additionally, the optimal result (26,804 kN) of Optimization V-1 based on EVRM is slightly higher than the optimal result (25,683 kN) of Optimization I-5 based on LHS.

In order to investigate the mechanism of the outstanding global optimizing ability of the proposed optimization framework based on EVRM, we compare the space-filling ability of sampling points of Optimization I-1 (81 LHS points) and Optimization V-1 (81 LPSS points). The space-filling diagrams of sampling points of Optimization I-1 and Optimization V-1 are plotted in Figures 5 to 8, including the relationships of h_{rj} and t_{rj}, h_{rn} and t_{rn}, t_{rj} and t_{rn}, h_{rj} and h_{rn}. Herein, we use space-filling factor *SFF* to evaluate the space-filling ability

$$SFF = A_{fill}/A_{all} \tag{5}$$

where A_{fill} stands for the area that sampling points fill and A_{all} stands for the area of the entire design space. When *SFF* value equals to 0.0, it indicates that the space-filling ability is the worst. The space-filing ability is better as the *SFF* value increases. When *SFF* value equals to 1.0, it indicates that the space-filling ability is the best.

To make the comparison clearer, the entire design space is divided into 81 equal portions, as shown in Figures 5 to 8. It can be observed that the *SFF* values of Optimization V-1 are higher than those of

Table 3. The design space and optimal results of prior optimizations based on candidate pairing strategies.

	t_s (mm)	t_{rj} (mm)	t_{rn} (mm)	h_{rj} (mm)	h_{rn} (mm)	N_{cj}	N_{cn}	N_{aj}	N_{an}	W (kg)	P_{cr} (kN)
Initial design	2.9	5.0	10.0	26.0	13.0	8	4	35	2	369	17766
Lower bound	2.5	3.0	3.0	15.0	6.0	3	1	20	1	–	–
Upper bound	5.5	12.0	12.0	30.0	15.0	9	4	50	4	369	–
Optimization II-1 (81 LPSS points)	5.5	3.8	4.9	29.0	13.2	6	1	50	1	369	26,377
Optimization III-1 (81 LPSS points)	4.8	6.8	5.0	27.4	9.5	6	2	49	1	369	26,940
Optimization IV-1 (81 LPSS points)	4.6	7.4	3.6	28.6	9.2	6	4	49	1	369	27,596
Optimization V-1 (81 LPSS points)	4.7	6.5	5.1	29.4	12.6	7	1	49	1	369	28,751
Optimization V-2 (64 LPSS points)	4.9	6.0	3.9	28.0	9.2	8	2	47	1	367	27,931
Optimization V-3 (100 LPSS points)	4.5	4.0	3.3	29.5	13.7	8	2	49	4	369	28,780

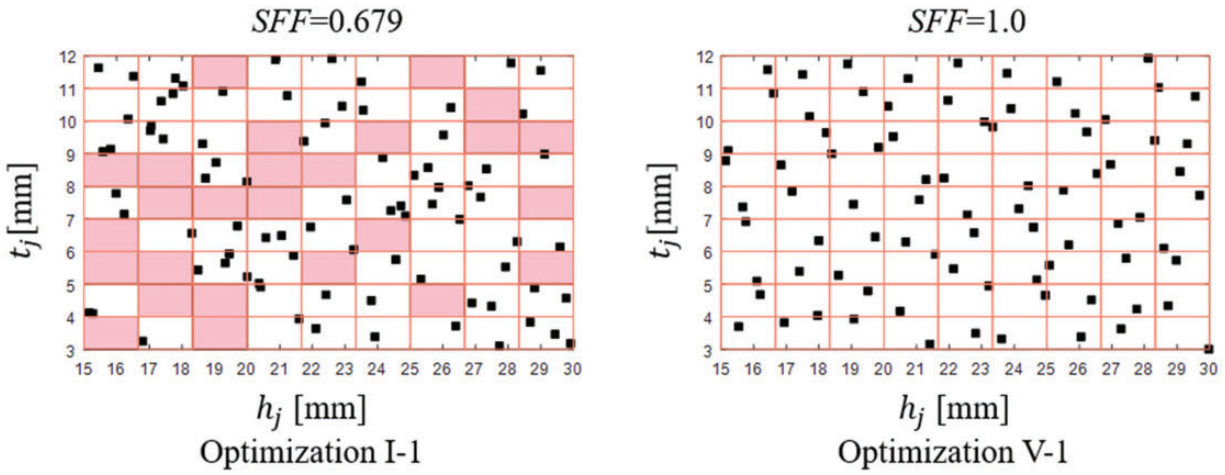

Figure 5. Space-filling diagrams of sampling points for variables h_{rj} and t_{rj}.

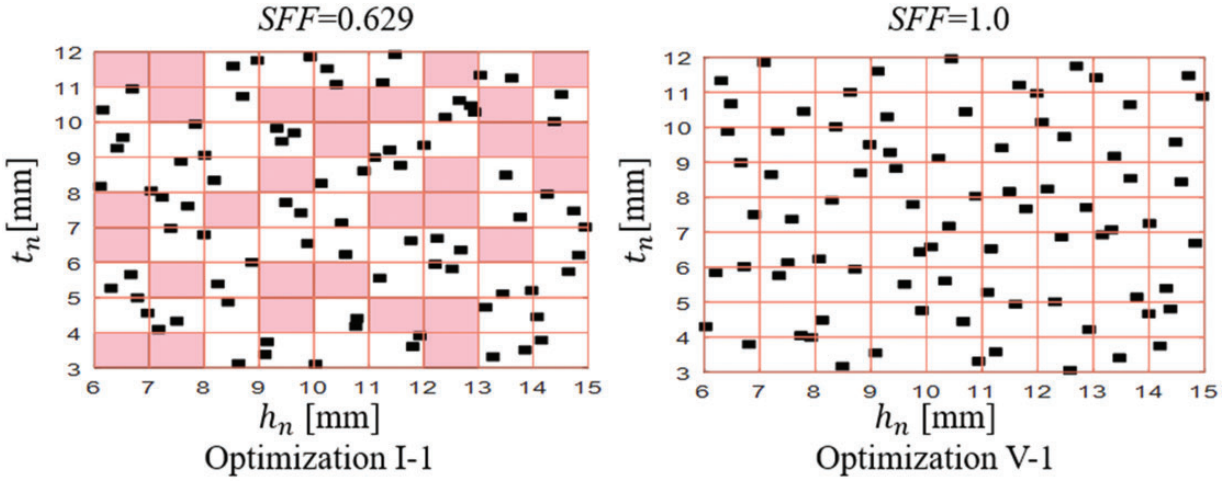

Figure 6. Space-filling diagrams of sampling points for variables h_{rn} and t_{rn}.

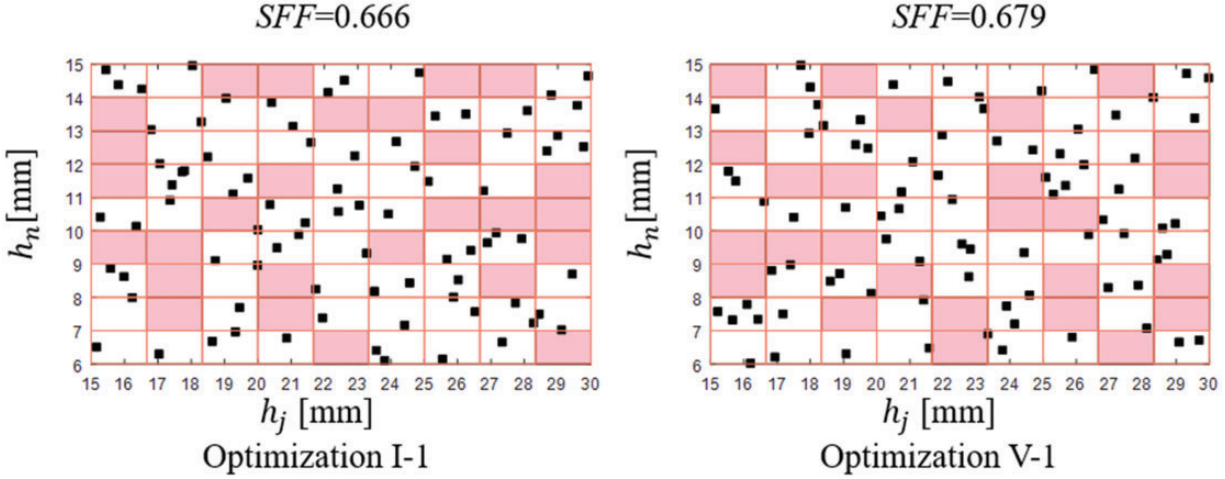

Figure 7. Space-filling diagrams of sampling points for variables h_{rj} and h_{rn}.

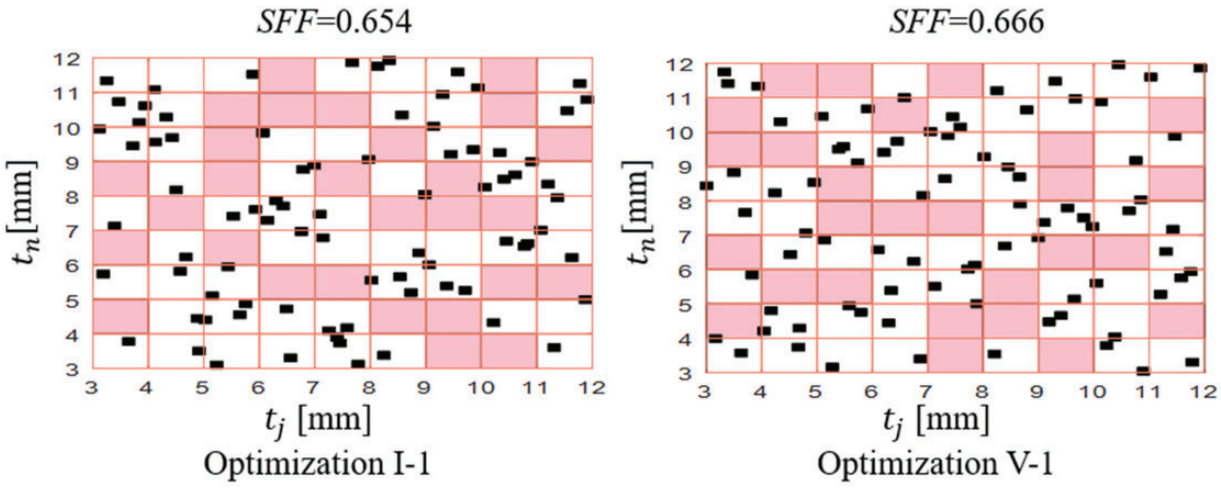

Figure 8. Space-filling diagrams of sampling points for variables t_{rj} and t_{rn}.

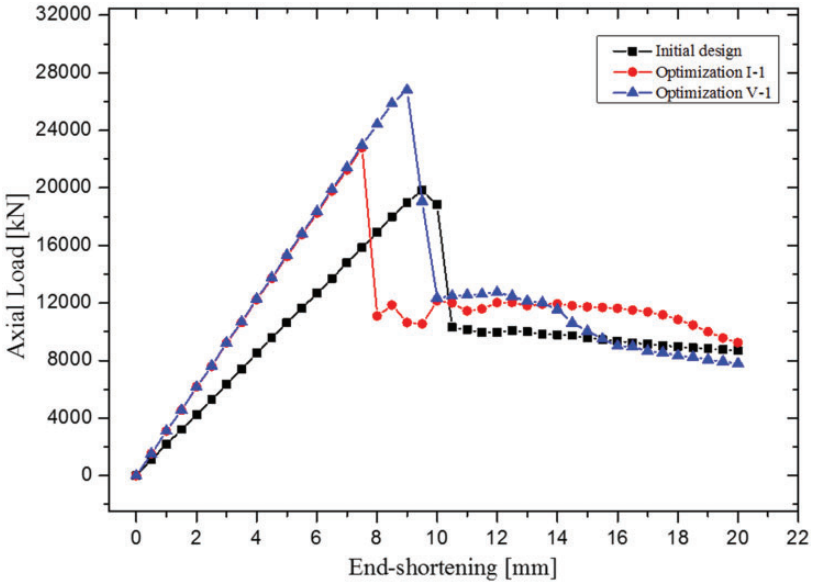

Figure 9. Load versus end-shortening curves of the initial design and optimal designs.

Optimization I-1, especially in Figures 5 and 6. Optimization I-1 does not well cover the sample space; conversely, Optimization V-1 has a better space-filling ability. In summary, by comparison of the space-filling results based on LHS and EVRM, it is worth noting that sampling points generated by EVRM are distributed more uniformly in the design space. In other words, EVRM has better space-filling ability than the traditional LHS method, particularly for the case that includes the mixture of main effects and variable interaction in high-dimensional complex system.

Discussions on the mechanism of the high load-carrying capacity of optimal results

In order to compare the load-carrying capacity of optimal results of the initial design, Optimization I-1 based on 81 LHS points and Optimization V-1 based on 81 LPSS points, their load versus end-shortening curves are plotted together in Figure 9. Note that the curve of the initial design has the smallest slope and the earliest onset of collapse. By contrast, the curve of Optimization V-1 has the largest slope and the onset of collapse is quite late. Then, the mechanism of the high load capacity of optimal results is investigated

Table 4. Effective stiffness coefficients of the initial design and optimization results.

	A_{11} (N/mm)	A_{22} (N/mm)	A_{12} (N/mm)	A_{66} (N/mm)	D_{11} (N·mm)	D_{22} (N·mm)	D_{12} (N·mm)	D_{66} (N·mm)
Initial design	579,264	464,095	95,022	113,545	23,527,229	16,771,531	232,415	1,062,786
Optimization I-1	591,963	687,099	164,643	192,541	8,957,169	17,437,572	1,362,288	1,727,856
Optimization V-1	606,285	649,672	154,519	181,382	24,059,141	33,873,455	1,090,596	1,620,956

from the point-of-view of effective stiffness coefficients. Herein, the NIAH method[66] is employed for the prediction of effective stiffness coefficients of hierarchical stiffened composite shells. The steps of NIAH are described as follows: firstly, a repeating unit cell (RUC) is divided from the whole model of hierarchical stiffened composite shells. The FEM model of the RUC is established in the finite element software, and the nodal displacement fields are applied to the RUC model. The first static analysis is run to obtain reaction nodal force vectors from output results. Then, above force vectors are imposed back to the initial RUC model, and the second static analysis under periodic boundary conditions is carried out to get characteristic displacement fields. Next, characteristic displacement fields are applied to the initial RUC model, and then the third static analysis is performed to obtain characteristic force fields. By the dot product of above values, effective extensional stiffness coefficients [A], effective bending-extension coupling stiffness coefficients [B], and bending stiffness coefficients [D] can be easily calculated.

Based on the NIAH method, effective extensional and bending stiffness coefficients of the initial design, Optimization I-1 and Optimization V-1 are calculated and corresponding results are listed in Table 4. By associating the curves in Figure 9 and the effective stiffness coefficients in Table 4, a conclusion can be drawn that the effective extensional and bending stiffness coefficients have significant influence on the load-carrying capacity of the hierarchical stiffened composite shell, which would reflect the shape differences of curves. When the design has higher effective extensional stiffness coefficients, its load versus end-shortening curve would have a larger slope, indicating higher axial stiffness of the hierarchical stiffened composite shell. When the design has higher effective bending stiffness coefficients, it would be more competitive in resisting the onset of the collapse, which would result in a higher collapse load. For the initial design, it has relatively low effective extensional stiffness coefficients. Therefore, its load versus end-shortening curve has the smallest slope. As for Optimization V-1 with the highest collapse load, it has high effective extensional and bending stiffness coefficients, and thus its curve has the largest slope and the onset of the collapse occurs quite late. Above all, it can be pointed out that high axial stiffness and bending stiffness are the main mechanism of the high load-carrying capacity of optimal results.

Conclusion

This paper proposes an optimization framework enhanced by EVRM that aims at improving the computational efficiency and global optimizing ability of the surrogate-based optimization of hierarchical stiffened composite shells against the buckling problem. The key idea of EVRM is to overcome the limitation of LPSS in determining the optimal pairing strategy for complex problems. By performing priori optimizations for candidate pairing strategies based on the low-fidelity analysis method, the optimal pairing strategy is determined with less computational cost. Based on the optimal pairing strategy, the surrogate-based optimization is carried out using the high-fidelity analysis method to obtain the optimal result. Compared with LHS, EVRM is more uniformly distributed in the design space and is more competitive in the space-filling ability. Next, optimization examples are performed to verify the effectiveness of the proposed optimization framework based on EVRM in comparison to the traditional optimization framework based on LHS. By comparison, it can be noted that when achieving an approximate global optimal solution, the proposed method enhanced by EVRM significantly reduces the total computational time by 76.3% than the traditional method based on LHS method. When using an approximate computational time, the optimal buckling result of the proposed method increases by 18.2% than that of the traditional method. Through the comparison of the optimal results of surrogate-based optimizations using LHS and EVRM, the advantage of EVRM in the surrogate-based optimization problem that includes the mixture of main effects and variable interaction in high dimensional complex system is highlighted. After validating the advantage of the proposed method in searching for the global optimal solution, the mechanism of the high load-carrying capacity of optimal results is further investigated by means of the NIAH method. By comparison

of effective stiffness coefficients of the initial design and optimal results, it is found that the high axial stiffness and bending stiffness contribute to achieving the high load-carrying capacity of hierarchical stiffened composite shells. The proposed buckling surrogate-based optimization framework can be easily extended to other types of complicated thin-walled structures, such as curvilinear stiffened shells and sandwich stiffened shells.

Declaration of conflicting interests

The author(s) declared no potential conflicts of interest with respect to the research, authorship, and/or publication of this article.

Funding

The author(s) disclosed receipt of the following financial support for the research, authorship, and/or publication of this article: This work was supported by China Postdoctoral Science Foundation (Grant No. 2019M651107), National Natural Science Foundation of China (Grant No. 11825202, No. 11772078), and LiaoNing Revitalization Talents Program (grant No. XLYC1802020). Additionally, we gratefully acknowledge the helpful discussions of Haixin Zhao and Zengcong Li from Dalian University of Technology.

ORCID iD

Kuo Tian https://orcid.org/0000-0002-2581-6984

References

1. Wagner H, Hühne C, Niemann S, et al. Robust knockdown factors for the design of cylindrical shells under axial compression: analysis and modeling of stiffened and unstiffened cylinders. *Thin-Walled Struct* 2018; 127: 629–645.
2. Zhang JX, Wang B, Niu F, et al. Design optimization of connection section for concentrated force diffusion. *Mech Based Des Struct* 2015; 43: 209–231.
3. Yazdani M and Rahimi GH. The effects of helical ribs' number and grid types on the buckling of thin-walled GFRP-stiffened shells under axial loading. *J Reinf Plast Compos* 2010; 29: 2568–2575.
4. Song B, Lyu D and Jiang J. Optimization of composite ring stiffened cylindrical hulls for unmanned underwater vehicles using multi-island genetic algorithm. *J Reinf Plast Compos* 2018; 37: 668–684.
5. Kidane S, Li G, Helms J, et al. Buckling load analysis of grid stiffened composite cylinders. *Compos Part B: Eng* 2003; 34: 1–9.
6. Shi SS, Sun Z, Ren M, et al. Buckling response of advanced grid stiffened carbon–fiber composite cylindrical shells with reinforced cutouts. *Compos Part B: Eng* 2013; 44: 26–33.
7. Li E. Fast cylinder variable-stiffness design by using Kriging-based hybrid aggressive space mapping method. *Adv Eng Softw* 2017; 114: 215–226.
8. Blom AW, Stickler PB and Gürdal Z. Optimization of a composite cylinder under bending by tailoring stiffness properties in circumferential direction. *Compos Part B: Eng* 2010; 41: 157–165.
9. Zhang H, Ding X, Dong X, et al. Optimal topology design of internal stiffeners for machine pedestal structures using biological branching phenomena. *Struct Multidiscip Optim* 2017; 57.
10. Wang D, Abdalla MM and Zhang W. Sensitivity analysis for optimization design of non-uniform curved grid-stiffened composite (NCGC) structures. *Compos Struct* 2018; 193: 224–236.
11. Chen L, Fan H, Sun F, et al. Improved manufacturing method and mechanical performances of carbon fiber reinforced lattice-core sandwich cylinder. *Thin-Walled Struct* 2013; 68: 75–84.
12. Sobhaniaragh B, Nejati M and Mansur WJ. Buckling modelling of ring and stringer stiffened cylindrical shells aggregated by graded CNTs. *Compos Part B: Eng* 2017; 124: 120–133.
13. Xiong J, Ghosh R, Ma L, et al. Sandwich-walled cylindrical shells with lightweight metallic lattice truss cores and carbon fiber-reinforced composite face sheets. *Compos Part A: Appl Sci Manuf* 2014; 56: 226–238.
14. Wang D, Abdalla MM, Wang ZP, et al. Streamline stiffener path optimization (SSPO) for embedded stiffener layout design of non-uniform curved grid-stiffened composite (NCGC) structures. *Comput Method Appl Mech Eng* 2018.
15. Zhao W and Kapania RK. Buckling analysis of unitized curvilinearly stiffened composite panels. *Compos Struct* 2016; 135: 365–382.
16. Yokozeki T, Shimizu Y, Ishii M, et al. Mechanical behavior in compression of skin-added X-lattice composite panel with corrugated ribs. *Compos Struct* 2017; 168: 863–871.
17. Wang P, Sun Ff, Fan Hl, et al. Retrofitting scheme and experimental research of severally damaged carbon fiber reinforced lattice-core sandwich cylinder. *Aerosp Sci Technol* 2016; 50: 55–61.
18. Jiang S, Sun FF and Fan HL. Multi-failure theory of composite orthogrid sandwich cylinder. *Aerosp Sci Technol* 2017; 70: 520–525.
19. Guo YL, Zhang YH, Zhu BL, et al. Experimental and numerical studies of instability mechanism and load resistance of rhombic grid hyperboloid-latticed shells under vertical load. *Eng Struct* 2018; 166: 167–186.
20. Kesel AB, Philippi U and Nachtigall W. Biomechanical aspects of the insect wing: an analysis using the finite element method. *Comput Biol Med* 1998; 28: 423–437.
21. Wang B, Tian K, Zhou CH, et al. Grid-pattern optimization framework of novel hierarchical stiffened shells allowing for imperfection sensitivity. *Aerosp Sci Technol* 2017; 62: 114–121.
22. Wang B, Hao P, Li G, et al. Optimum design of hierarchical stiffened shells for low imperfection sensitivity. *Acta Mech Sin* 2014; 30: 391–402.

23. Hao P, Wang B, Li G, et al. Hybrid optimization of hierarchical stiffened shells based on smeared stiffener method and finite element method. *Thin-Walled Struct* 2014; 82: 46–54.
24. Zhao YN, Chen M, Yang F, et al. Optimal design of hierarchical grid-stiffened cylindrical shell structures based on linear buckling and nonlinear collapse analyses. *Thin-Walled Struct* 2017; 119: 315–323.
25. Wang B, Tian K, Zhao HX, et al. Multilevel optimization framework for hierarchical stiffened shells accelerated by adaptive equivalent strategy. *Appl Compos Mater*. 2017; 24: 575–592.
26. Du B, Chen LM, Wu W, et al. A novel hierarchical thermoplastic composite honeycomb cylindrical structure: fabrication and axial compressive properties. *Compos Sci Technol* 2018; 164: 136–145.
27. Li M, Sun F, Lai C, et al. Fabrication and testing of composite hierarchical isogrid stiffened cylinder. *Compos Sci Technol* 2018; 157: 152–159.
28. Wu H, Lai C, Sun F, et al. Carbon fiber reinforced hierarchical orthogrid stiffened cylinder: fabrication and testing. *Acta Astronaut* 2018; 145: 268–274.
29. Zhang B, Chen H, Zhao Z, et al. Blast response of hierarchical anisogrid stiffened composite panel: considering the damping effect. *Int J Mech Sci* 2018; 140: 250–259.
30. Quinn D, Murphy A, McEwan W, et al. Stiffened panel stability behaviour and performance gains with plate prismatic sub-stiffening. *Thin-Walled Struct* 2009; 47: 1457–1468.
31. Quinn D, Murphy A, McEwan W, et al. Non-prismatic sub-stiffening for stiffened panel plates - stability behaviour and performance gains. *Thin-Walled Struct* 2010; 48: 401–413.
32. Quinn D, Murphy A and Glazebrook C. Aerospace stiffened panel initial sizing with novel skin sub-stiffening features. *Int J Struct Stab Dyn* 2012; 12: 1250060.
33. Houston G, Quinn D, Murphy A, et al. Design rules for stiffened panel buckling containment features. *Thin-Walled Struct* 2017; 116: 69–81.
34. Sim CH, Park JS, Kim HI, et al. Postbuckling analyses and derivations of knockdown factors for hybrid-grid stiffened cylinders. *Aerosp Sci Technol* 2018; 82–83: 20–31.
35. Sim CH, Kim HI, Lee YL, et al. Derivations of knockdown factors for cylindrical structures considering different initial imperfection models and thickness ratios. *Int J Aeronaut Space Sci* 2018; 19: 626–635.
36. Wang C, Xu Y and Du J. Study on the thermal buckling and post-buckling of metallic sub-stiffening structure and its optimization. *Mater Struct* 2016; 49: 4867–4879.
37. Tian K, Wang B, Hao P, et al. A high-fidelity approximate model for determining lower-bound buckling loads for stiffened shells. *Int J Solids Struct* 2018; 148: 14–23.
38. Wang B, Du K, Hao P, et al. Numerically and experimentally predicted knockdown factors for stiffened shells under axial compression. *Thin-Walled Struct* 2016; 109: 13–24.
39. Wang B, Ma XT, Hao P, et al. Improved knockdown factors for composite cylindrical shells with delamination and geometric imperfections. *Compos Part B: Eng* 2018; 165: 314–323.
40. Lanzi L. A numerical and experimental investigation on composite stiffened panels into post-buckling. *Thin-Walled Struct* 2004; 42: 1645–1664.
41. Hao P, Wang B, Tian K, et al. Integrated optimization of hybrid-stiffness stiffened shells based on sub-panel elements. *Thin-Walled Struct* 2016; 103: 171–182.
42. Hao P, Wang B, Tian K, et al. Fast procedure for non-uniform optimum design of stiffened shells under buckling constraint. *Struct Multidisc Optim* 2017; 55: 1503–1516.
43. Wang B, Zhu S, Hao P, et al. Buckling of quasi-perfect cylindrical shell under axial compression: a combined experimental and numerical investigation. *Int J Solids Struct* 2018; 130: 232–247.
44. Tian K, Wang B, Zhou Y, et al. Proper-orthogonal-decomposition-based buckling analysis and optimization of hybrid fiber composite shells. *AIAA J* 2018; 56: 1723–1730.
45. Liang K and Sun Q. Reduced-order modeling analysis of shell structures buckling using a co-rotational solid-shell element. *Aerosp Sci Technol* 2017; 70: 435–444.
46. Liang K and Ruess M. Nonlinear buckling analysis of the conical and cylindrical shells using the SGL strain based reduced order model and the PHC method. *Aerosp Sci Technol* 2016; 55: 103–110.
47. Sun JB, Lim CW, Xu XS, et al. Accurate buckling solutions of grid-stiffened functionally graded cylindrical shells under compressive and thermal loads. *Compos Part B: Eng* 2016; 89: 96–107.
48. Tian K, Wang B, Zhang K, et al. Tailoring the optimal load-carrying efficiency of hierarchical stiffened shells by competitive sampling. *Thin-Walled Struct* 2018; 133: 216–225.
49. Xu Z, Lu X and Law KH. A computational framework for regional seismic simulation of buildings with multiple fidelity models. *Adv Eng Softw* 2016; 99: 100–110.
50. Zhou Q, Yang Y, Jiang P, et al. A multi-fidelity information fusion metamodeling assisted laser beam welding process parameter optimization approach. *Adv Eng Softw* 2017; 110: 85–97.
51. Park JS. Optimal Latin-hypercube designs for computer experiments. *J Stat Plan Infer* 1994; 39: 95–111.
52. Rubinstein RY and Kroese DP. *Simulation and the Monte Carlo method*. New York: John Wiley & Sons, 2016.
53. Zhang JX and Shields MD. Probability measure changes in Monte Carlo simulation. *Probab Eng Mech* 2018.
54. Helton JC and Davis FJ. Latin hypercube sampling and the propagation of uncertainty in analyses of complex systems. *Reliab Eng Syst Saf* 2003; 81: 23–69.
55. Zhang JX and Shields MD. On the quantification and efficient propagation of imprecise probabilities resulting from small datasets. *Mech Syst Signal Process* 2018; 98: 465–483.
56. Zhang JX and Shields MD. The effect of prior probabilities on quantification and propagation of imprecise probabilities resulting from small datasets. *Comput Method Appl Mech* 2018; 334: 483–506.

57. Stein M. Large sample properties of simulations using Latin hypercube sampling. *Technometrics* 1987; 29: 143–151.
58. Shields MD, Teferra K, Hapij A, et al. Refined stratified sampling for efficient Monte Carlo based uncertainty quantification. *Reliab Eng Syst Saf* 2015; 142: 310–325.
59. Shields MD and Zhang JX. The generalization of Latin hypercube sampling. *Reliab Eng Syst Saf* 2016; 148: 96–108.
60. Whitley D, Rana S and Heckendorn RB. The island model genetic algorithm: on separability, population size and convergence. *J Comput Inform Technol* 1999; 7: 33–47.
61. Cui Y, Wang LF and Ren JY. Multi-functional SiC/Al composites for aerospace applications. *Chinese J Aeronaut* 2008; 21: 578–584.
62. Qian L, Pang X, Zhou J, et al. Theoretical model and finite element simulation on the effective thermal conductivity of particulate composite materials. *Compos Part B: Eng* 2017; 116: 291–297.
63. Singh J. Fabrication characteristics and tribological behavior of Al/SiC/Gr hybrid aluminum matrix composites: a review. *Friction* 2016; 4: 191–207.
64. Rikards R, Abramovich H, Kalnins K, et al. Surrogate modeling in design optimization of stiffened composite shells. *Compos Struct* 2006; 73: 244–251.
65. Myers RH, Montgomery DC and Anderson-Cook CM. *Response surface methodology: process and product optimization using designed experiments*. New York: John Wiley & Sons, 1995.
66. Cai YW, Xu L and Cheng GD. Novel numerical implementation of asymptotic homogenization method for periodic plate structures. *Int J Solids Struct* 2014; 51: 284–292.